Nanoscale

PAPER

View Article Online
View Journal | View Issue

Check for updates

Cite this: *Nanoscale*, 2022, **14**, 14956

Printing nanoparticle-based isotropic/anisotropic networks for directional electrical circuits†

Sisi Chen,[a,b] Qi Pan,*[a,b] Tingqing Wu,[a,b] Hongfei Xie,[a,b] Tangyue Xue,[a,c] Meng Su*[a,b] and Yanlin Song *[a,b]

Received 15th July 2022,
Accepted 17th September 2022

DOI: 10.1039/d2nr03892g

rsc.li/nanoscale

With the demand for integrated nanodevices, anisotropic conductive films are one type of interconnection structure for electronic components, which have been widely used for improving the integration of the system in printed circuit boards. This work presents a template-assisted printing strategy for the fabrication of nanoparticle-based networks with multi electrical properties. By manipulating the microfluid behavior under the guidance of the grid-shaped template, the continuity of liquid bridges can be precisely controlled in two directions. The isotropous circuits with crossbar paths, discrete paths as well as unidirectional paths are obtained, which achieve the switching of on/off states in the circuits. This work demonstrates a new type of directional circuits by the template-assisted printing method, which provides an effective fabrication strategy for electrical components and integrated systems.

Published on 28 1401. Downloaded on 01/04/1403 12:14:13 ..

Introduction

Circuits serve as the medium for information communication and power transmission in the microelectronic system.[1–5] The printed circuit boards (PCBs) assemble thousands of electronic components to realize the integration of different functions, such as computing,[6,7] displays,[8,9] and sensing.[10–12] Functional materials and structures with large sizes and fixed properties hardly meet the needs of integrated micro-devices.[13–17] The fine-pitch interconnect technology has become one of the important research areas for the microelectronics industry to meet the increasing demands of downsizing, functionalization, and integration.[18–21] Anisotropic materials can achieve different functions in different directions.[22–24] As one type of interconnection materials for electronic components, anisotropic conductive films (ACFs) possess a specific directional conductivity.[25,26] ACFs consist of conductive particles dispersed in insulation materials, which is insufficient in conductivity and integration.[27,28] The ultimate direction of interfacing in electronics is the direct integration of miniaturized electrodes on the high-resolution circuit. Novel interconnection structures for ACFs, such as the electrode networks with directional conductivity, provide a large number of conductive paths, which could meet the demands of performance and integration in electronic systems.[29,30]

Printing strategies facilitate the fabrication in microelectronic systems due to the precise design of the structure from microscale to nanoscale.[31–37] Current printing techniques, such as inkjet printing[38–40] and screen printing,[41–43] enable the fabrication of architectures with the desired pattern, but still hardly ensure the production of devices with the demanded precision and accuracy.[44,45] On the other hand, these methods require specific printing plates or complicated printing paths to achieve the preparation of different isotropic/anisotropic patterns, which leads to increasing manufacturing costs.[46–48] Moreover, due to the capillary attraction from the heteromorphic ink droplet, printed isotropic/anisotropic patterns usually result in non-uniform structures,[49] which causes the poor performance of directional conductivity. It is critical to develop an efficient printing method to fabricate the electrode network with controllable and directional conductivity.

This work demonstrates a template-assisted printing strategy to fabricate isotropic/anisotropic electrode networks in a simplified process. The grid-shaped template with a height difference between longitudinal walls and transverse walls is scribed on purpose. The Ag nanoparticle (Ag NP)-based ink is divided into transverse and longitudinal liquid bridges under the guidance of the grid-shaped template. Through manipulating the evolution of the shrinkage of the ink, the continuity and geometry of liquid bridges in two directions can be well designed, forming three types of paths (crossbar paths, uni-

[a]*Key Laboratory of Green Printing, CAS Research/Education Center for Excellence in Molecular Sciences, Institute of Chemistry, Chinese Academy of Sciences (ICCAS), Beijing Engineering Research Center of Nanomaterials for Green Printing Technology, Beijing National Laboratory for Molecular Sciences (BNLMS), Beijing 100190, P. R. China. E-mail: panqipanqi@iccas.ac.cn, sumeng1988@iccas.ac.cn, ylsong@iccas.ac.cn*
[b]*University of Chinese Academy of Sciences, Beijing 100049, P. R. China*
[c]*School of Materials Science and Engineering, Zhengzhou University, Zhengzhou 450001, P. R. China*
† Electronic supplementary information (ESI) available. See DOI: https://doi.org/10.1039/d2nr03892g

This journal is © The Royal Society of Chemistry 2022

Published on 28 1401. Downloaded on 01/04/1403 12:14:13 ..

directional paths, and close-loop paths) for the assembly of Ag NPs. As a result, the isotropic/anisotropic circuit networks, including crossbar circuits, unidirectional circuits, and discrete circuits, are obtained. The printed isotropic/anisotropic networks exhibit diverse electrical characteristics in different directions. The remarkable anisotropy resistance ratio over 10^{11} demonstrates excellent performance and achieves effective control of LED displays. This work provides a new prototype for isotropic/anisotropic circuits through the template-assisted printing strategy, which can be applied to integrated microelectronic systems.

Experimental

Materials preparation

Silicon wafers (2-inch diameter, N doped, ⟨100⟩ oriented, 525 μm thick) were patterned using the dicing saw machine (Heyan Technology, China). The width of the blade was 18 μm. The groove shape showed a longitudinal depth of 19.24 μm and a transverse depth of 15.89 μm. Then, the groove-shaped silicon wafer was treated with hydrophobic molecules (1*H*,1*H*,2*H*,2*H*-perfluorodecyltriethoxysilane, CAS 101947-16-4) in a decompression environment at 25 °C for 1 h and then heated at 80 °C for 3 h, yielding the reproducible homogeneous hydrophobic surfaces. Next, 40 mL of poly(dimethylsiloxane) (PDMS) precursor mixed with the initiator (Sylgard 184, Dow Corning Company, USA) was carefully dropped onto the groove-shaped silicon wafer and heated at 70 °C for 1 h to prepare the grid-shaped PDMS template with a longitudinal height of 17.76 μm and a transverse height of 14.52 μm. Silicon oxide substrates were washed in the ultrasonic device for 5 min with acetone, ethanol, and deionized water and dried with high purity nitrogen. PDMS template with a contact angle of 78.5 ± 0.4° was obtained after the plasma treatment. The silicon oxide substrate without treatment exhibited a contact angle of 50.1 ± 0.5° (Fig. S1†). Silver nanoparticles (Ag NPs) with an average particle size of 40 nm were synthesized according to the literature.[50] To monitor the flow behavior during the printing process, sodium fluorescein (a green fluorescent dye) was added to the Ag NP dispersion. The fluorescence images were obtained at the excitation wavelength of 488 nm.

Generation of isotropic/anisotropic structures

A grid-shaped template was placed horizontally. Ag NP ink (5–60 mg mL^{-1} Ag NPs and 1 mg mL^{-1} sodium dodecyl sulfate (SDS), J&K Scientific Ltd Beijing, China) was carefully dropped onto the template and covered by a prepared silicon oxide substrate. Weights with fixed mass are attached to the template to apply external pressure. The template, droplet, and substrate consisted of a sandwich structure. The grid-shaped template induced the retraction of transverse and longitudinal liquid bridges. Continuous or dispersed liquid bridges were determined by the applied pressure. By manipulating the directional shrinkage of the suspension, the liquid flow organized Ag NPs into designed structures. The whole system was kept at 60 °C for 3 h. When the temperature was low (<40 °C), the solvents evaporated slowly, which caused Ag NPs to move slowly and then led to the unsuccessful shrinkage of the liquid bridges. The liquid bridges shrank fast at a high temperature (>80 °C). The fragile liquid bridges increased the deformities in the isotropic/anisotropic structures. It was suitable at the temperature of 40–80 °C. In this study, the whole system was kept at 60 °C. After the liquid completely dried, the template was removed by physical peeling. Then, the fabricated circuits based on Ag NPs were sintered at 200 °C for 1 h.

Characterization and measurement

The optical images and fluorescent microscopy images were acquired by an optical microscope (Nikon LV100ND) that was coupled to a charge-coupled device camera (Vision Engineering Co.). The contour graphs of the silicon wafer and PDMS template were acquired by a profilometer (ContourGT-K). Contact angles were measured using a contact angle measurement device (OCA20, Data Physics, Germany) with latex droplets (water, 2 μL) deposited on the substrates. The structures of crossbar circuits (CC), unidirectional circuits (UC), and discrete circuits (DC) were investigated by a scanning electron microscope (SEM, S4800, Japan) at the accelerating voltage of 5.0 kV. The electrical measurement was performed by a Keithley 4200-SCS semiconductor system and a Suss PM5 analytical probe station in a clean and shielded box under ambient conditions. Two tungsten probes were placed in contact with the printed Ag lines. The impressed voltage was applied to detect the corresponding current. The current signal was read by the Keithley 4200-SCS semiconductor system with a Suss PM5 analytical probe station. The resistance (R) of the printed Ag lines is calculated by $R = US/IL$, where U is the applied voltage, S is the section area of the Ag line, I is the current signal, and L is the length of the Ag line. Specifically, four separate 100 nm-thick Au electrodes (A–D) were deposited around the fabricated circuits through a shadow mask using a high vacuum thermal evaporation system (PATOR, ATT010).

Results and discussion

In this work, we propose a template-assisted printing platform for patterning isotropic/anisotropic structures (Fig. 1a). Grooves are scribed on a smooth silicon wafer by the dicing saw machine. The gird-shaped PDMS template is obtained by replicating the groove pattern with transverse and longitudinal depth differences (Fig. S2†). For fabricating isotropic/anisotropic structures, a template-liquid-substrate sandwich printing system is constructed. In the printing system, the nanomaterial-loaded liquid is divided into transverse and longitudinal liquid bridges, which guide the nanomaterials to assemble into specific structures in different directions. The designed isotropic/anisotropic architectures can be fabricated by regulating the liquid flow in the transverse and longitudinal directions. To manipulate the liquid flow in two directions separ-

Published on 28 1401. Downloaded on 01/04/1403 12:14:13 ..

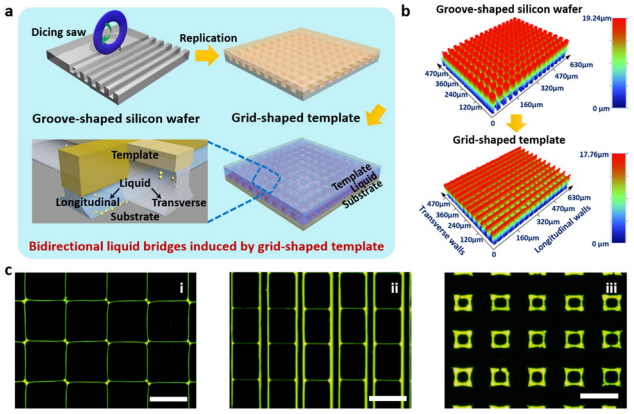

Fig. 1 Printing isotropic/anisotropic structures with the designed template. (a) Schematic illustration of patterning micro/nanostructures by the template-assisted printing strategy. Crossbar liquid bridges can be formed under the guidance of the grid-shaped template. (b) 3D contour graphs of groove-shaped silicon wafer and replicated grid-shaped template. The heights of transverse and longitudinal walls are 17.76 μm and 14.52 μm, respectively. (c) Fluorescent microscopy images of printing isotropic/anisotropic paths. (i) Crossbar path arrays; (ii) unidirectional path arrays; (iii) closed-loop arrays. Scale bar: 40 μm.

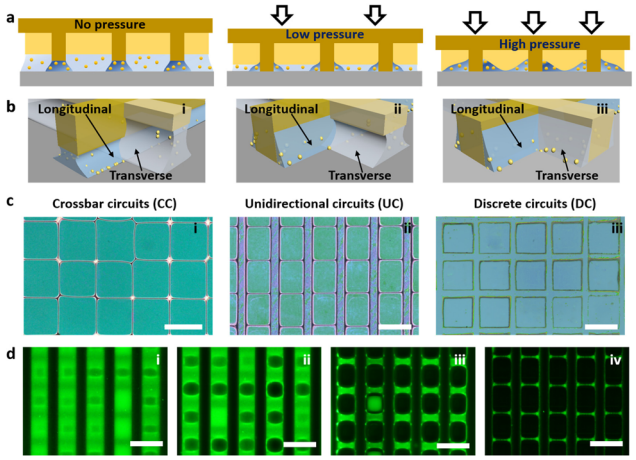

Fig. 2 Controllable template-assisted printing process and printed isotropic/anisotropic structures. (a) The printing system, including the gap between the template and the substrate, and the filling state of the liquid, is affected by the attached pressure. (b) Three types of liquid bridges induced by the pressure of the printing system. (i) Crossbar liquid bridges; (ii) unidirectional liquid bridges; (iii) discrete liquid bridges. Continuous and separate liquid bridges lead the nanomaterials assembling on the top and sides of the template, respectively. (c) Optical images of the three types of circuits. (i) Crossbar circuits (CC); (ii) unidirectional circuits (UC); (iii) discrete circuits (DC). Scale bar: 40 μm. (d) *In situ* fluorescent microscopy observation of flow behavior in the UC printing process. Scale bar: 100 μm.

ately, the groove-shaped silicon wafer is designed with a height difference on the micro-scale. As a result, the replicated template shows a longitudinal wall height of 17.76 μm and a transverse wall height of 14.52 μm, respectively. (Fig. 1b and Fig. S3†). The gap between the substrate and the template can manipulate the formation of isotropic/anisotropic liquid bridges. The continuity of liquid bridges in two directions determines the paths in the final arrays. By manipulating the formation of paths in the printing process, the isotropic/anisotropic arrays can be obtained. Fig. 1c shows the three typical isotropic/anisotropic arrays, including the crossbar path arrays, unidirectional path arrays, and closed-loop arrays. These patterns provide designable configurations for isotropic/anisotropic arrays, which can be used primarily for high-density connections in electrical or optical devices.

The grid-shaped template serves as guidance to build liquid bridges, which directs the ink to locate in the desired position. The difference between liquid bridges in the transverse and longitudinal directions induces multiple configurations of arrays. In the printing process, the shape of liquid bridges is affected by the gap between the substrate and the template. Fig. 2a shows the controllable template-assisted printing process. Crossbar liquid bridges, unidirectional liquid bridges, and discrete liquid bridges are achieved by regulating the applied pressure. Specifically, the attached pressure adjusts the gap between the template and the substrate and further affects the flow behavior in the printing system, which influences the formation of liquid bridges and the assembly of functional nanomaterials. In this case, uniform Ag NPs with an average particle size of 40 nm are used as the functional ink (Fig. S4†). There is sufficient space between the template and the substrate to support liquid bridges under the condition of no applied pressure. The template can induce liquid bridge contraction in two directions. With the evaporation of the solvent, the liquid film is split and pinned onto the top of the template, forming crossbar paths (Fig. 2b i). As a consequence, nanomaterials assemble both transversely and longitudinally, forming crossbar circuits (CC) (Fig. 2c i). When proper pressure is applied, the walls with large heights (the longitudinal walls) are attached to the substrate, resulting in liquid bridges remaining on both sides of the walls in the longitudinal direction. As a consequence, nanomaterial-loaded droplets shrink along the longitudinal walls. On the other hand, liquid bridges form on the top of transverse walls, and nanoparticles aggregate at the position of liquid bridges. Accordingly, the transverse path is split by longitudinal walls (Fig. 2b ii), forming unidirectional circuits (UC), as shown in Fig. 2c ii. As the pressure increases, the template in two directions adheres to the substrate. The liquid film is split, and liquid bridges in two directions are blocked at the same time, which leads to separated liquid bridges (Fig. 2b iii) and discrete circuits (DC) (Fig. 2c iii). The fabrication of directional circuits can be realized by the accurate control of the continuity of liquid bridges in multiple directions. Furthermore, isotropic/anisotropic circuits can be obtained on the same template through precise control of liquid bridges in the printing process, benefitting from the flexibility of the template-assisted printing method.

In order to describe the printing process of anisotropic circuits, *in situ* fluorescent microscope observation is carried out (Fig. 2d). At first, the liquid film is filled in the template-assisted printing system. As the solvent evaporates, liquid

This journal is © The Royal Society of Chemistry 2022

Published on 28 1401. Downloaded on 01/04/1403 12:14:13 ..

shrinks on the sides of longitudinal walls and anchors on the top of transverse walls. Longitudinal liquid bridges remain continuous, while transverse liquid bridges are divided by longitudinal walls. Then, unidirectional paths are formed. By manipulating liquid bridges under the designed template and controllable gap, isotropic/anisotropic circuits are fabricated in a simplified step. This manufacturing methodology provides an effective way to pattern diverse architectures without complicated fabrication.

In the printing system, there are two main factors that influence the final structures. The concentration of the Ag NP ink affects the quality of the wires in the circuits. On the other hand, the pressure applied to the printing system regulates liquid bridges, which determines the circuit configuration. To obtain the desired circuits, precise control is investigated by adjusting the concentration of Ag NPs and the applied pressure (Fig. 3a). The width and continuity of printed lines can be tuned by the concentration of Ag NPs. As the concentration of Ag NPs increases from 5 mg mL^{-1} to 60 mg mL^{-1}, the width of printed lines can be manipulated from 650 nm to 2 μm (Fig. S5†). A high concentration solution prevents the liquid from being extruded and maintains the gap. Therefore, continuous liquid bridges tend to fabricate continuous lines. When the concentration of the Ag NP ink decreases, the gap is more easily eliminated, and the printed lines are more likely to be discrete. In addition, the micro-scale gap between the template and the substrate is affected by the applied pressure directly. Continuous liquid bridges in two directions are formed under a low pressure. As a consequence, Ag NPs tend to congregate in CC. When the applied pressure increases, longitudinal walls adhere to the substrate and squeeze out the liquid, resulting in the formation of discrete transverse liquid bridges and continuous longitudinal liquid bridges. This leads to the fabrication of UC. Perfect UC can be obtained at 20–40 mg mL^{-1} of Ag NPs with an applied pressure of 1–3 kPa. When the applied pressure is high (>3 kPa), the template is attached to the substrate, leaving split liquid bridges in both transverse and longitudinal directions. The pattern of DC can be obtained in this situation. Fig. 3b shows magnified SEM images of CC, UC, and DC. Applied pressure not only determines the continuity of liquid bridges, but also affects the location of liquid bridges and the configuration of printed lines. The Ag NP ink can be filled into the gap between the template and the substrate and assembled on the top of the template under the applied pressure of less than 1 kPa. Therefore, the side view of the printed line is an isosceles triangle (Fig. 3c). With an increased applied pressure, the Ag NP ink is squeezed and tends to gather on the sides of the template, forming an inclined triangle instead (Fig. 3d). Ag NPs are packed tightly regardless of the position of the assembled nanoparticles. The silver lines in both CC and UC exhibit satisfying electrical conductivity of 1.6×10^{-7} Ω m and 1.3×10^{-7} Ω m after being sintered at 200 °C for 1 h (Fig. 3e).

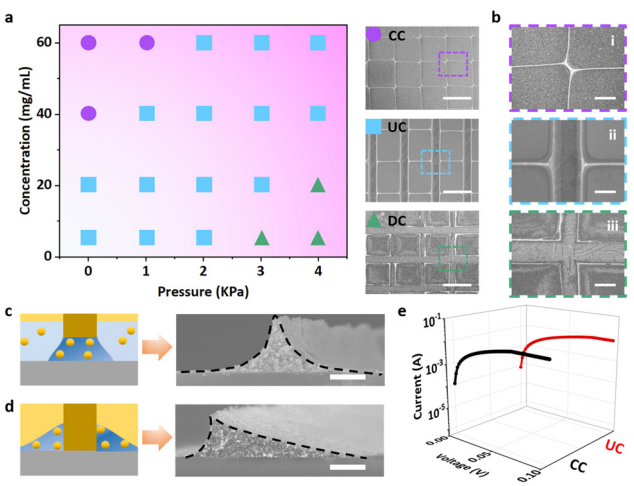

Fig. 3 Precise fabrication and characteristics of the isotropic/anisotropic structures. (a) The final structure plot of the isotropic/anisotropic structure is the function of the concentration of Ag NPs and applied pressure. Perfect UC circuits can be obtained at 20–40 mg mL^{-1} with an applied pressure of 1–3 kPa. Scale bar: 40 μm. (b) Magnified scanning electron microscope (SEM) images of the CC, UC, and DC in (a). Scale bar: 10 μm. (c) Schematic and SEM images of assembled Ag NPs on the top of the template under no pressure. Scale bar: 1 μm. (d) Schematic and SEM images of assembled Ag NPs on the sides of the template. Scale bar: 1 μm. (e) The conductivity of conducting units of CC and UC.

Diverse architectures with directional configurations can be adapted to interconnect micro-electrical circuits to achieve isotropic/anisotropic conductivity. The longitudinal and transverse conductivity of the isotropic/anisotropic networks is characterized. When the applied voltage is 0.05 V, CC exhibits superb conductivity in both transverse and longitudinal directions (the corresponding current is 6.30×10^{-3} A). DC is non-conductive in two directions (the corresponding current is 3.48×10^{-15} A). UC is conductive in the longitudinal direction (the corresponding current is 7.84×10^{-3} A) and non-conductive in the transverse direction (the corresponding current is 1.35×10^{-14} A) (Fig. 4a). The on/off ratio reaches up to 10^{11}, benefiting from the anisotropic structure. The printed silver lines exhibit uniform resistance and line width, which is significant for stable performance in circuits (Fig. 4b). The fabricated CC, UC, and DC meet the demand for direct integration of miniaturized devices in micro-scale circuits. To demonstrate the electrical performance of isotropic/anisotropic networks in light-emitting diode (LED) circuits, four electrode interfaces (A–D) are loaded.

The circuits exhibit different conducting states when accessed to different electrodes of UC on the circuit networks (Fig. 4c). When UC is connected by electrode A and electrode C in the longitudinal direction, the printed circuit is conductive, and the LED is on (Fig. 4d i). When UC is accessed to electrodes B and electrode D (or electrode A and electrode B), the device serves as the breaker, and the LED goes off (Fig. 4d ii and iii). When CC is accessed to electrode A and electrode C, electrode B and electrode D, or electrode A and electrode B, the LED is on for its continuous printed networks in two directions (Fig. S6†). DC is non-conductive when accessed in circuits with any electrodes because the device with discrete lines

Published on 28 1401. Downloaded on 01/04/1403 12:14:13 ..

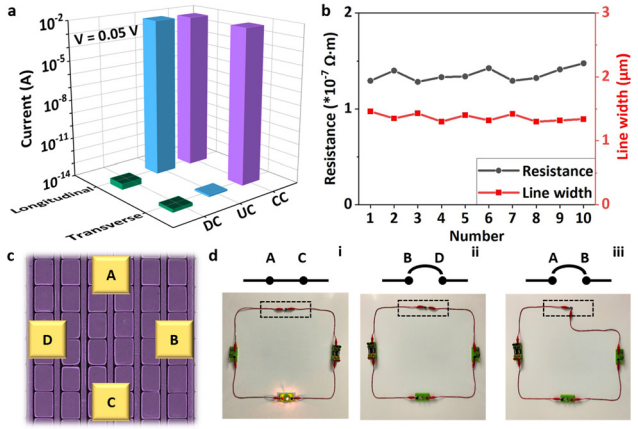

Fig. 4 Performance of the printed isotropic/anisotropic networks. (a) Transverse and longitudinal current is mapped in CC, UC, and DC at the voltage of 0.05 V. CC exhibits conducting characteristics in both transverse and longitudinal circuits. UC exhibits conducting characteristics in transverse circuits and non-conducting characteristics in longitudinal circuits. DC exhibits non-conducting characteristics in neither transverse nor longitudinal circuits. (b) The uniformity of conductive circuits. (c) Tested UC and the four evaporated electrodes A–D. (d) Application of anisotropic networks in LED circuits.

acts as the breaker and the LED is off (Fig. S7†). The distinctive electrical properties of isotropic/anisotropic circuits suggest great potential as electrical components.

Conclusions

In summary, we demonstrate a template-assisted printing strategy to fabricate isotropic/anisotropic networks with multi electrical properties. Guided by the grid-shaped template, isotropic/anisotropic paths are achieved. Owing to the height difference between longitudinal walls and transverse walls in the template, liquid bridges exhibit adjustable continuity in two directions. The Ag NPs loaded liquid flow can be precisely regulated both in the transverse and longitudinal directions. Under specific applied pressure in the printing process, three types of circuit arrays, including CC, UC, and DC, are successfully prepared. The printed isotropic/anisotropic networks exhibit diverse electrical characteristics in different directions. A remarkable anisotropy resistance ratio of over 10^{11} is achieved, realizing effective control of the LED display. This template-assisted printing strategy enables a feasible and flexible strategy for manufacturing isotropic/anisotropic circuits, rendering promising applications for integrated electrical systems in miniaturized devices.

Author contributions

Qi Pan, Meng Su and Yanlin Song proposed the original idea of the template-assisted printing strategy. Sisi Chen, Qi Pan, and Meng Su designed and carried out the experiments. Tingqing Wu, Hongfei Xie, and Tangyue Xue participated in the discussion and provided suggestions. Sisi Chen, Qi Pan, Meng Su, and Yanlin Song wrote the manuscript with support from all co-authors. Yanlin Song conceived and supervised the project.

Conflicts of interest

There are no conflicts to declare.

Acknowledgements

Yanlin Song, Meng Su, and Qi Pan are grateful for the financial support of the National Natural Science Foundation of China (Grant No. 22075296, 52103310, 91963212, and 51961145102), the National Key R&D Program of China (Grant No. 2018YFA0208501), Beijing Nova Program from Beijing Municipal Science & Technology Commission (Grant No. Z201100006820037, and Z211100002121001), the China Postdoctoral Science Foundation (Grant No. 2020TQ0325 and 2020M680679), Beijing National Laboratory for Molecular Sciences (Grant No. BNLMS-CXXM-202005).

References

1 A. Kumar, M. Gupta and R. Singh, *Nat. Electron.*, 2022, **5**, 261–262.
2 S. Liu, D. S. Shah and R. Kramer-Bottiglio, *Nat. Mater.*, 2021, **20**, 851–858.
3 Z. Wang, X. Xia, M. Zhu, X. Zhang, R. Liu, J. Ren, J. Yang, M. Li, J. Jiang and Y. Liu, *Adv. Funct. Mater.*, 2022, **32**, 2108336.
4 S. Cho, Y. Yun, S. Jang, Y. Ra, J. H. Choi, H. J. Hwang, D. Choi and D. Choi, *Nano Energy*, 2020, **71**, 104584.
5 C. Wan, P. Cai, X. Guo, M. Wang, N. Matsuhisa, L. Yang, Z. Lv, Y. Luo, X. J. Loh and X. Chen, *Nat. Commun.*, 2020, **11**, 4602.
6 Z. Zhou, K. Chen, X. Li, S. Zhang, Y. Wu, Y. Zhou, K. Meng, C. Sun, Q. He, W. Fan, E. Fan, Z. Lin, X. Tan, W. Deng, J. Yang and J. Chen, *Nat. Electron.*, 2020, **3**, 571–578.
7 Y. Yang, X. Wei, N. Zhang, J. Zheng, X. Chen, Q. Wen, X. Luo, C.-Y. Lee, X. Liu, X. Zhang, J. Chen, C. Tao, W. Zhang and X. Fan, *Nat. Commun.*, 2021, **12**, 4876.
8 W. Yang, Y. Zhu, Z. Jia, L. He, L. Xu, J. Meng, M. Tahir, Z. Zhou, X. Wang and L. Mai, *Adv. Energy Mater.*, 2020, **10**, 2001873.
9 W.-J. Song, M. Kong, S. Cho, S. Lee, J. Kwon, H. B. Son, J. H. Song, D.-G. Lee, G. Song, S.-Y. Lee, S. Jung, S. Park and U. Jeong, *Adv. Funct. Mater.*, 2020, **30**, 2003608.
10 Y. Song, J. Min, Y. Yu, H. Wang, Y. Yang, H. Zhang and W. Gao, *Sci. Adv.*, 2020, **6**, eaay9842.
11 X. Li, X. Huang, J. Mo, H. Wang, Q. Huang, C. Yang, T. Zhang, H.-J. Chen, T. Hang, F. Liu, L. Jiang, Q. Wu, H. Li, N. Hu and X. Xie, *Adv. Sci.*, 2021, **8**, 2100827.
12 D. Jung, C. Lim, H. J. Shim, Y. Kim, C. Park, J. Jung, S. I. Han, S.-H. Sunwoo, K. W. Cho, G. D. Cha, D. C. Kim,

This journal is © The Royal Society of Chemistry 2022

Published on 28 1401. Downloaded on 01/04/1403 12:14:13 ..

J. H. Koo, J. H. Kim, T. Hyeon and D.-H. Kim, *Science*, 2021, **373**, 1022–1026.
13 S. Das, A. Sebastian, E. Pop, C. J. McClellan, A. D. Franklin, T. Grasser, T. Knobloch, Y. Illarionov, A. V. Penumatcha, J. Appenzeller, Z. Chen, W. Zhu, I. Asselberghs, L.-J. Li, U. E. Avci, N. Bhat, T. D. Anthopoulos and R. Singh, *Nat. Electron.*, 2021, **4**, 786–799.
14 Y.-Q. Zheng, Y. Liu, D. Zhong, S. Nikzad, S. Liu, Z. Yu, D. Liu, H.-C. Wu, C. Zhu, J. Li, H. Tran, J. B.-H. Tok and Z. Bao, *Science*, 2021, **373**, 88–94.
15 A. G. Kelly, J. O'Reilly, C. Gabbett, B. Szydłowska, D. O'Suilleabhain, U. Khan, J. Maughan, T. Carey, S. Sheil, P. Stamenov and J. N. Coleman, *Small*, 2022, **18**, 2105996.
16 I. Hwang, M. Seong, H. Yi, H. Ko, H.-H. Park, J. Yeo, W.-G. Bae, H. W. Park and H. E. Jeong, *Adv. Funct. Mater.*, 2020, **30**, 2000458.
17 S. Han, K.-W. Seo, W. Kim, T.-S. Kim and J.-Y. Lee, *Nanoscale*, 2021, **13**, 4543–4550.
18 S. Wang, J. Xu, W. Wang, G.-J. N. Wang, R. Rastak, F. Molina-Lopez, J. W. Chung, S. Niu, V. R. Feig, J. Lopez, T. Lei, S.-K. Kwon, Y. Kim, A. M. Foudeh, A. Ehrlich, A. Gasperini, Y. Yun, B. Murmann, J. B. H. Tok and Z. Bao, *Nature*, 2018, **555**, 83–88.
19 J. A. Strong, V. V. Talanov, M. E. Nielsen, A. C. Brownfield, N. Bailey, Q. P. Herr and A. Y. Herr, *Nat. Electron.*, 2022, **5**, 171–177.
20 J. Deng, X. Li, M. Li, X. Wang, S. Shao, J. Li, Y. Fang and J. Zhao, *Nanoscale*, 2022, **14**, 4679–4689.
21 W. Li, L. Li, Q. Sun, X. Liu, M. Kanehara, T. Nakayama, J. Jiu, K. Sakamoto and T. Minari, *Chem. Eng. J.*, 2021, **416**, 127644.
22 S. E. Kim, F. Mujid, A. Rai, F. Eriksson, J. Suh, P. Poddar, A. Ray, C. Park, E. Fransson, Y. Zhong, D. A. Muller, P. Erhart, D. G. Cahill and J. Park, *Nature*, 2021, **597**, 660–665.
23 J. Chen, X. Liu, Y. Tian, W. Zhu, C. Yan, Y. Shi, L. B. Kong, H. J. Qi and K. Zhou, *Adv. Mater.*, 2022, **34**, 2102877.
24 L. Meng, R. Bian, C. Guo, B. Xu, H. Liu and L. Jiang, *Adv. Mater.*, 2018, **30**, 1706938.
25 X. Li, Q. Ma, J. Tian, X. Xi, D. Li, X. Dong, W. Yu, X. Wang, J. Wang and G. Liu, *Nanoscale*, 2017, **9**, 18918–18930.
26 G. Gaál, M. L. Braunger, V. Rodrigues, A. Riul Jr. and H. L. Gomes, *Adv. Electron. Mater.*, 2021, **7**, 2100255.
27 H. Hwang, M. Kong, K. Kim, D. Park, S. Lee, S. Park, H.-J. Song and U. Jeong, *Sci. Adv.*, 2021, **7**, eabh0171.
28 Y.-G. Park, J. Jang, H. Kim, J. C. Hwang, Y. W. Kwon and J.-U. Park, *Adv. Electron. Mater.*, 2022, **8**, 2101034.
29 D. H. Kim, H. G. Yoo, S. M. Hong, B. Jang, D. Y. Park, D. J. Joe, J.-H. Kim and K. J. Lee, *Adv. Mater.*, 2016, **28**, 8371–8378.
30 Z. Zhang, Y. Wang, Z. Chen, D. Xu, D. Zhang, F. Wang and Y. Zhao, *J. Nanobiotechnol.*, 2022, **20**, 117.
31 Y. Li, Z. Zhang, M. Su, Z. Huang, Z. Li, F. Li, Q. Pan, W. Ren, X. Hu, L. Li and Y. Song, *Nanoscale*, 2018, **10**, 22374–22380.
32 M. Su and Y. Song, *Chem. Rev.*, 2021, **122**, 5144–5164.
33 Q. Pan, S. Chen, M. Su, P. Li, Z. Zhang, X. Hu, G. Chen, Z. Huang, B. Chen, S. Chen and Y. Song, *Adv. Opt. Mater.*, 2020, **8**, 2000370.
34 B. Elder, R. Neupane, E. Tokita, U. Ghosh, S. Hales and Y. L. Kong, *Adv. Mater.*, 2020, **32**, 1907142.
35 R. T. Su, J. X. Wen, Q. Su, M. S. Wiederoder, S. J. Koester, J. R. Uzarski and M. C. McAlpine, *Sci. Adv.*, 2020, **6**, eabc9846.
36 M. Su, F. Qin, Z. Zhang, B. Chen, Q. Pan, Z. Huang, Z. Cai, Z. Zhao, X. Hu, D. Derome, J. Carmeliet and Y. Song, *Angew. Chem., Int. Ed.*, 2020, **59**, 14234–14240.
37 L. Li, W. Li, Q. Sun, X. Liu, J. Jiu, M. Tenjimbayashi, M. Kanehara, T. Nakayama and T. Minari, *Small*, 2021, **17**, 2101754.
38 I. Kim, B. Ju, Y. Zhou, B. M. Li and J. S. Jur, *ACS Appl. Mater. Interfaces*, 2021, **13**, 24081–24094.
39 C. Xiang, L. Wu, Z. Lu, M. Li, Y. Wen, Y. Yang, W. Liu, T. Zhang, W. Cao, S.-W. Tsang, B. Shan, X. Yan and L. Qian, *Nat. Commun.*, 2020, **11**, 1646.
40 F. Molina-Lopez, T. Z. Gao, U. Kraft, C. Zhu, T. Öhlund, R. Pfattner, V. R. Feig, Y. Kim, S. Wang, Y. Yun and Z. Bao, *Nat. Commun.*, 2019, **10**, 2676.
41 G. Zhu, P. Ren, J. Yang, J. Hu, Z. Dai, H. Chen, Y. Li and Z. Li, *Nano Energy*, 2022, **98**, 107327.
42 S. Zheng, H. Wang, P. Das, Y. Zhang, Y. Cao, J. Ma, S. Liu and Z.-S. Wu, *Adv. Mater.*, 2021, **33**, 2005449.
43 H. Eynaki, M. A. Kiani and H. Golmohammadi, *Nanoscale*, 2020, **12**, 18409–18417.
44 Z. Xia, V. Mishukova, S. Sollami Delekta, J. Sun, J. S. Sanchez, J. Li and V. Palermo, *Nanoscale*, 2021, **13**, 3285–3294.
45 S. Abdolhosseinzadeh, R. Schneider, A. Verma, J. Heier, F. Nuesch and C. J. Zhang, *Adv. Mater.*, 2020, **32**, 2000716.
46 S. H. Lee, J. Kim, J. H. Shin, H. E. Lee, I.-S. Kang, K. Gwak, D.-S. Kim, D. Kim and K. J. Lee, *Nano Energy*, 2018, **44**, 447–455.
47 P. Zhang, Q. Wang, R. Guo, M. Zhang, S. Wang, C. Lu, M. Xue, J. Fan, Z. He and W. Rao, *Mater. Horiz.*, 2019, **6**, 1643–1653.
48 K. Zhao, S. Li, M. Huang, X. Shi, G. Zheng, C. Liu, K. Dai, C. Shen, R. Yin and J. Z. Guo, *Chem. Eng. J.*, 2019, **358**, 924–935.
49 D. Ershov, J. Sprakel, J. Appel, M. A. C. Stuart and J. V. D. Gucht, *Proc. Natl. Acad. Sci. U. S. A.*, 2013, **110**, 9220–9224.
50 P.-Y. Silvert, R. Herrera-Urbina, N. Duvauchelle, V. Vijayakrishnan and K. T. Elhsissen, *J. Mater. Chem.*, 1996, **6**, 573–577.